Spatial dispersion contribution to second harmonic generation in inversion-symmetric materials

Hendradi Hardhienata,[1,*] Adalberto Alejo-Molina,[2] Muhammad Danang Birowosuto,[3,4] Amirreza Baghbanpourasl,[5] and Husin Alatas[1]

[1]*Theoretical Physics Division, Department of Physics, IPB University, Meranti Avenue, Wing S Building, Dramaga Campus of IPB, Bogor 16680, West Java, Indonesia*

[2]*Center for Research in Engineering and Applied Science (CIICAp), Institute for Research in Pure and Applied Science (IICBA), UAEM Cuernavaca, Morelos 62209, Mexico*

[3]*CNRS International NTU THALES Research Alliances/UMI 3288 (CINTRA), Research Techno Plaza, 50 Nanyang Drive, Border X Block, Level 6, Singapore 637553, Singapore*

[4]*Department of Renewable Energy Engineering, Universitas Prasetiya Mulya, Kavling Edutown I.1, Jl. BSD Raya Utama, BSD City, Tangerang 15339, Indonesia*

[5]*Center for Surface- and Nanoanalytics, Johannes Kepler University, Altenberger Straße 69, 4040 Linz, Austria*

(Received 23 November 2020; revised 17 February 2021; accepted 17 February 2021; published 8 March 2021)

It is well known that second harmonic generation (SHG) from dipoles within the bulk vanishes in inversion-symmetric semiconductor materials as a consequence of parity symmetry. Hence SHG is then ascribed in the form of either surface dipole effects or bulk-related electric quadrupole or magnetic dipole effects. By incorporating the redefined spatial dispersion into the simplified bond-hyperpolarizability model, we show that the SHG spatial dispersion contribution for Si(001) and Si(111) facet orientations can be reformulated by a third-rank tensor containing one independent parameter, namely, the complex SHG spatial dispersion hyperpolarizability. Our results show that certain unexplained rotational anisotropy SHG intensity features for different incoming light wavelengths or optical penetration depths can be well reproduced only if the contribution from spatial dispersion is incorporated.

DOI: 10.1103/PhysRevB.103.125410

I. INTRODUCTION

The recent progress in surface science techniques capable of probing surfaces *in situ* and in a nondestructive way has renewed interest in linear and nonlinear optical techniques such as second harmonic generation (SHG). This interest has been accompanied by theoretical efforts to model the measured data, either interpreting them in a classical phenomenological picture [1–3] or taking into account quantum mechanics by involving transitions between initial and final states [4–9]. Especially for SHG, the interpretation of the various nonlinear contributions to explain experimental data is sometimes controversial. Several authors [10–12] claim that part of the SHG response arises from the surface and bulk quadrupoles or from magnetic dipole effects, whereas others are mainly considering surface contributions [13,14].

To our knowledge, discussions regarding the effect of spatial dispersion in nonlinear optics remain limited, even in high-symmetry centrosymmetric materials such as silicon (Si). Here, we define spatial dispersion as the spatial variation of the incident fundamental field inside the medium as discussed by Peng *et al.* [12]. Guyot-Sionnest and Shen [10] argue that the electric dipole terms vanish for SHG, and the authors consider magnetic dipoles and electric quadrupoles as sources for bulk-related SHG. Although they mention spatial dispersion in the form of a gradient term in their work, they also state that for cubic crystals (e.g., Si, Cu, Ge) the field gradient term only applies to the surface and the gradient contribution should vanish inside the bulk. We will later explain that this bulk gradient contribution does not vanish.

So far, a direct proof that spatial dispersion from an incoming light decay can contribute significantly to rotational anisotropy SHG (RASHG) intensity experimental data remains elusive although it has been shown more recently using classical electrodynamics calculation that spatial dispersion can also contribute to SHG if an electric field gradient is present [12]. Still, its exact contribution relative to the other SHG sources (surface dipolar and bulk quadrupolar) has never been investigated explicitly and is often left out in the analysis of bulk dipole transitions in materials with inversion symmetry [15–17]. A new hope of uncovering the spatial dispersion contribution in inversion-symmetric materials arises from the formulation of the simplified bond-hyperpolarizability model (SBHM) first proposed by Powell *et al.* [14] by expanding the Ewald-Oseen extinction theorem in linear optics to nonlinear optics [18]. Assuming that the RASHG intensity originates from anharmonic oscillating dipoles along the Si covalent bonds, they successfully explained the origin of the RASHG data for vicinal Si(111) using only two complex hyperpolarizability independent parameters, which proves to be a major simplification of earlier phenomenological models [1,2,19]. An effort was also made to introduce terrace and step hyperpolarizability to model Si(111) using the SBHM with

*hendradi@apps.ipb.ac.id

different offcut directions and different offcut magnitudes [20]. In addition, the SBHM was later improved to explain that the RASHG intensity profile from other silicon orientations can indeed be modeled more precisely if other nondipolar sources are involved such as a quadrupolar contribution [18]. Using the SBHM, we were able to model a surface RASHG experiment for a nonvicinal Si(111) surface with satisfactory results [21]. Indeed, it has also been shown using arbitrary input polarization that bulk quadrupolar effects contribute significantly to the total RASHG intensity of certain Si surfaces [22,23] and are related to the first-order derivatives of the microscopic response function [24]. The validity of the SBHM was further confirmed with the ability to model experimental RASHG data from zinc blende samples confirming the existence of bulk dipole radiation as the dominant source of SHG [25]. We also showed recently that second harmonic generation in wurtzite structures, e.g., ZnO, with surface twin boundaries can also be described using the SBHM [26] as well as third harmonic generation (THG) from within the ZnO bulk [27].

In this paper we derive an expression for the SHG spatial dispersion tensor using the SBHM. The connection between the third-rank susceptibility tensor obtained from the SBHM and that obtained from group theory (GT) was first established for SHG and THG in Si structures [28,29]. The results show that when Kleinman symmetry can be applied, the nonzero tensor from GT can be derived via the SBHM, where the latter requires either the same or fewer independent parameters than GT. Thus the SBHM is generally simpler than phenomenological models that apply GT to calculate the tensor. It will be shown later in this paper that our previous work on applying the SBHM to electric-field-induced second harmonic (EFISH) experimental results from a metal oxide semiconductor (MOS) is useful for the calculation of the spatial dispersion third-rank tensor [30] with an important note that the third-order nonlinear susceptibility tensor related to EFISH can be reduced into a second-order nonlinear susceptibility tensor. In this paper we will apply some of the line of thinking in our previous EFISH work to show that spatial dispersion can also be reinterpreted and analyzed in the form of an effective second-order nonlinear SHG polarization. We therefore arrange this paper as follows: In Sec. II we provide an argument as to how SHG spatial dispersion can be interpreted and how it can occur for a certain diamond facet orientation. In Sec. III we discuss how this interpretation can be incorporated in the theoretical framework of Peng *et al.* [12]. In Sec. IV we discuss experimental evidence of a spatial dispersion contribution using the SBHM for a Si(111) facet. Finally, a summary is provided in Sec. V.

II. SHG SPATIAL DISPERSION IN SILICON

It is well known from standard nonlinear optics theory that materials with inversion symmetry are described by potentials with even powers of the coordinates (i.e., r^2, r^4, etc.). Because a SHG contribution providing a response to an incident field oscillating with frequency ω could originate, due to inversion symmetry, only from forces which are cubic in a component of $\vec{r}$, this effect has been directly excluded. Analytically, the quantum mechanical expression for each tensor element of the second-order susceptibility is [31]

$$\chi_{ijk}^{\mathrm{SHG}} = \frac{Ne^3}{\varepsilon_0 \hbar^2} \sum_{n,n'} \left(\frac{\langle j\rangle_{0n}\langle k\rangle_{nn'}\langle i\rangle_{n'0}}{(\omega_{n0}-\omega)(\omega_{n'0}-2\omega)} + \frac{\langle k\rangle_{0n}\langle i\rangle_{nn'}\langle j\rangle_{n'0}}{(\omega_{n0}-\omega)(\omega_{n'0}+\omega)} + \frac{\langle i\rangle_{0n}\langle j\rangle_{nn'}\langle k\rangle_{n'0}}{(\omega_{n0}+2\omega)(\omega_{n'0}+\omega)} \right). \quad (1)$$

Here, i, j, k denote x, y, z; N is the density of oscillators; and each sum runs over all intermediate states n, n'. For a symmetric potential (e.g., fcc and bcc lattices with a single atom basis) the product of an uneven number of excitations cannot close the loop back to the original state so that $\chi_{ijk}^{\mathrm{SHG}}$ is zero. Locally, however, a diamond (111) facet orientation is due to the atoms' tetrahedral bonding, intrinsically inversion asymmetric. This asymmetry can be observed by using a pictorial representation of the tetrahedral hybridized sp^3 wave functions [Fig. 1(a)], by displaying the *ab initio* potential along the ⟨111⟩ direction [Fig. 1(b)], or by plotting the potential within the (111) plane as an equicontour plot [Fig. 1(c)]. The potential has been calculated with the density functional theory implementation of VASP 5.2 using the generalized gradient approximation (GGA). The interaction between the four electrons and the Si ion is described by the projector augmented wave technique [32]. The constructed potential describing fourfold ionized Si and four electrons is rather strong ($\simeq -120$ eV). The calculated electron energies, however, are of the order of a few eV, and therefore the electrons "feel" the asymmetry of the potential. Including the exchange correlation part makes the potential landscape even more asymmetric.

In contrast, the *ab initio* potential parallel to a Si(100) surface is inversion symmetric, and so an electric field vector within this plane cannot excite SHG. However, because the polarization of the electric field can be in an arbitrary direction to the bonds, each Si atom will produce, for an arbitrary polarization, a SHG response. Also, for the case of Si(111), the SHG response will be minor because two neighboring Si atoms form a symmetric entity, if there is no perturbation. So, in all static or long-wavelength-limit effects, the SHG response of two neighboring Si atoms cancels, as well as for certain symmetries between the perturbing electric field and the crystallographic arrangement [e.g., normal incidence on Si(110) or Si(100)].

In the general case, however, when the amplitude of the electric field is different on both atom sites, the two responses will not add up fully destructively and will produce in the far field a measurable signal. A strength variation of the electric field could occur either through strong (asymmetric) focusing or, which is discussed beneath, by the intrinsic absorption of the fundamental wave, when it propagates into the material. Since the ratio between the incoming beam radius and its penetration depth is 150 : 1, the contribution of the longitudinal spatial dispersion is much higher than the

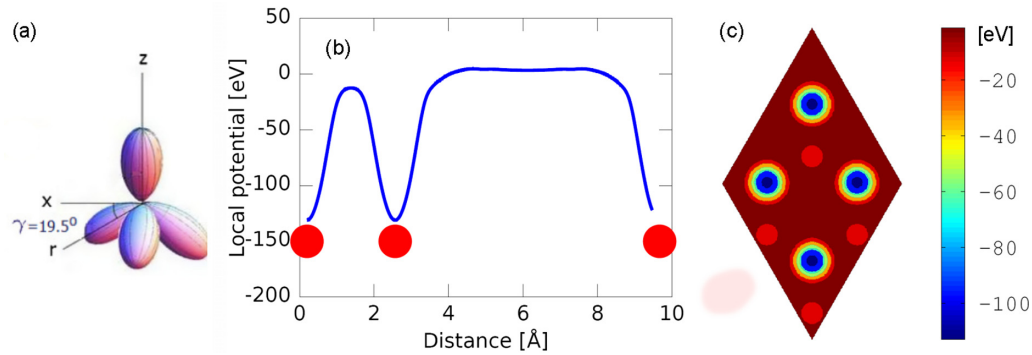

FIG. 1. (a) Plot of the probability density for the sp^3 hybridized wave functions for Si(111). (b) *Ab initio* potential for Si(111) along the [111] direction. (c) Contour plot of the *ab initio* potential for Si in the (111) plane. The red dots represent the positions of the Si atoms.

transverse part [33]. Therefore we can assume that the spatial dispersion of the field is significant along the optical axis (z axis). The effect of a varying amplitude of the *macroscopic* electric field can be described by either employing spatially dispersive (nonlocal) models, which means that the dielectric function depends on the wave vector and the frequency as in Ref. [34], or, as done recently, deriving within a classical bond model that the spatial dispersion is proportional to the gradient of the macroscopic electric field along the bond [12]. Using bonds instead of the lattice positions disguises the symmetry properties of the underlying lattice and requires the use of classical mechanics. Therefore we will proceed by explicitly specifying the spatial dependence of the macroscopic electric fields. If a wave impinges perpendicular to, e.g., silicon with a (111) orientation [see Fig. 2(a)], the perturbation through the electric field $\vec{E}$ can be significant.

Si(111), and its atoms, can be described in a simple picture by four equivalent covalent bonds with a sequence of layers, which are alternatingly bound by one up bond or by three down bonds to the next layer [see Fig. 2(b)]. For our model it is not significant whether we imagine the bonds as rigid, such that the electrons can only move along the bond direction [14] or as sp^3-hybridized orbitals [35], or as extended coherent wave functions, describing the probability density for finding the electron in a given spatial interval. The electronic

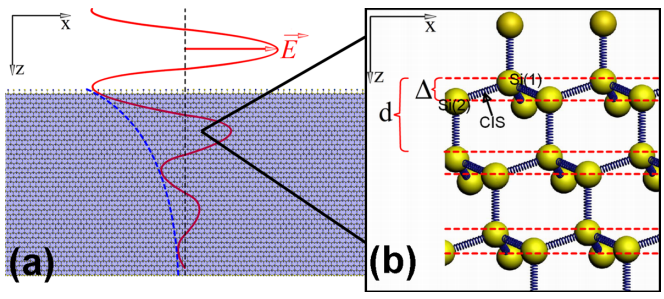

FIG. 2. (a) The incoming electric field decays along the propagation direction. (b) Layers are shown where one Si atom [Si(1)] is covalently bound to one from above and to three Si atoms underneath, where one is called Si(2). The center of inversion symmetry (CIS) is located in the middle between Si(1) and Si(2).

probability density is the same for positions around Si(1) and those around Si(2), which are at slightly different z positions (Fig. 2). The nonlinear spatial dispersion polarization for a single atom or layer, either Si(1) or Si(2), is then derived by

$$P_i^{\mathrm{SD},2\omega} = \frac{\varepsilon_0}{2}\sum_{jk}\chi_{ijk}^{\mathrm{SD}}(2\omega;\omega,\omega)E_j(\omega)E_k(\omega), \tag{2}$$

where χ_{ijk}^{SD} stands for the specific coefficient of the nonlinear hyperpolarizability of a single Si atom or layer. The nonlinear hyperpolarizability yields for a single Si(111) tetrahedron a finite contribution as has been found before for a single sp^3 orbital [35]. For the case of the later-discussed SBHM [14], χ_{ijk}^{SD} can be easily found by setting the up and the down hyperpolarizabilities equal in the cited reference.

When the fundamental field penetrates through the bulk, it decays with a complex wave vector $k = \omega\tilde{n}/c$ and an absorption coefficient $\alpha_\omega/2$, given by $\alpha_\omega = \frac{4\pi n_i}{\lambda_0}$, where λ_0 is the vacuum wavelength and n_i is the imaginary part of the refractive index $\tilde{n}$, connected to the dielectric function $\epsilon(\omega)$ by $\epsilon(\omega) = \tilde{n}(\omega)^2$. Because the exciting field decays along z due to absorption, the response of the bonds of Si(1) does not fully cancel the contribution of the lower atom Si(2). It has to be mentioned that even for the case that the photon energy is smaller than half the band gap, the occurrence of SHG implies absorption of the linear wave. For a bond length in Si of $\simeq$2.35 Å the period d of the slabs is $\simeq$3.16 Å, and the normal distance Δ between the Si(1) and Si(2) atoms is $\simeq$0.8 Å. We calculate the difference of the radiated SHG field for one slab just beneath the surface ($z = 0^+$) as the coherent superposition of the Si(1) and Si(2) atoms:

$$\begin{aligned}
C_{(1)} &= (\mathrm{Re}[e^{ik_\omega z}])^2 e^{-\alpha_\omega z}\mathrm{Re}[e^{ik_{2\omega}z}]e^{-\alpha_{2\omega}z/2},\\
C_{(2)} &= \left(\mathrm{Re}[e^{ik_\omega(z+\Delta)}]\right)^2 e^{-\alpha_\omega(z+\Delta)}\\
&\quad\times \mathrm{Re}\left[e^{ik_{2\omega}(z+\Delta)}\right]e^{-\alpha_{2\omega}(z+\Delta)/2},\\
P_{i\mathrm{SD}}^{\mathrm{slab},2\omega} &= \frac{\varepsilon_0}{2}\sum_{jk}\chi_{ijk}^{\mathrm{SD}}(2\omega;\omega,\omega)(C_{(1)}-C_{(2)})E_j^0(\omega)E_k^0(\omega),
\end{aligned} \tag{3}$$

where the first equation yields the response of Si(1) at z and the second equation yields the response of Si(2) at depth $z+\Delta$. We explicitly use real fields in the nonlinear process.

The exponential decaying terms in the field have to be squared in the nonlinear process, yielding the absorption coefficient. Also the backward propagating wave with twice the fundamental frequency is damped, which is then detected in vacuum or air. The third equation makes explicit use of spatial dispersion, i.e., the field dependence, and E_j^0 denotes the transmitted space independent fundamental electric field amplitude at $z = 0^+$, having put the decaying terms into $(C_{(1)} - C_{(2)})$.

Extending the calculation to the full bulk is straightforward by splitting the crystal into slabs with Si atoms at position 1 or 2, numerating only each double layer by n, replacing $z \to n \cdot d$, and summing the fields coherently over all slabs. The procedure is similar to the Ewald-Oseen ansatz [36] for linear optics with the difficulty of using real fields. The outside detected field or intensity is the coherent superposition of the field originating from the surface and the field originating from the Si(111) bulk: $I = \frac{1}{2}c\varepsilon_0|E_{\text{surf}} + E_{\text{bulk}}|^2$.

Here, we do not treat the field produced by the surface E_{surf}, where specific models on reconstruction and electronic states would have to be considered. The bulk contribution, however, can be calculated analytically, by using computer algebra systems, and also numerically. To determine its relative magnitude, we proceed—in order to show the physics more clearly—by neglecting the phase of the field [$\simeq$ sign in Eq. (4)]. This analytic procedure is approximately correct for the case of rather high absorption coefficients, when the field is overcritically damped:

$$P_{i\text{SD}}^{2\omega,\text{bulk}} = \frac{\varepsilon_0}{2}\sum_{jk}\chi_{ijk}^{\text{SD}}(2\omega;\omega,\omega)\sum_{n=1}^{\infty}(C_{(1,n)} - C_{(2,n)})E_j^0(\omega)E_k^0(\omega)$$
$$\simeq \frac{\varepsilon_0}{2}\frac{\left(1 - e^{-\Delta(\alpha_{2\omega}/2+\alpha_\omega)}\right)}{e^{d(\alpha_{2\omega}/2+\alpha_\omega)} - 1}\sum_{jk}\chi_{ijk}^{\text{SD}}(2\omega;\omega,\omega)E_j^0(\omega)E_k^0(\omega). \tag{4}$$

A modified absorption coefficient $\alpha_{\text{SHG}} = \alpha_{2\omega}/2 + \alpha_\omega$ governs the contribution of the bulk to SHG. For very large, experimentally not achievable, α_{SHG} (penetration depth of just a few angstroms) the formula above yields a vanishing bulk SHG contribution, leaving only the surface effect. As discussed before, in the general case the surface and the bulk field should be added coherently. However, already for harmonic excitation close to the E_1 transition in Si, α_{SHG} is of the order of $\simeq$0.02 Å^{-1}, equivalent to penetration depths of just $\simeq$120 Å for the exciting wave and $\simeq$60 Å for the frequency-doubled wave. For $\alpha_{\text{SHG}} = 0.02$ Å^{-1} the bulk contribution can give rise to a quarter of the contribution of a single bond for the case of setting the first unperturbed atom as the one with three down bonds, or even three-quarters if it has three up bonds. It will be shown later that the bulk contribution from quadrupoles and spatial dispersion can roughly account for half the SHG intensity for a large incoming light penetration depth. By this calculation it is clear that the bulk contribution cannot be neglected when using SHG as a surface analytical tool and can have the same magnitude as the contribution arising from the surface.

For very small absorption coefficients α_{SHG}, i.e., almost transparent materials, we find an additional condition, similar to Manley-Rowe relations, which provides the conservation of energy: Using Eq. (4), we use an expansion of the denominator and obtain as leading term $\frac{\chi^{\text{SD}}\Delta}{d}$, equal to $\chi^{\text{SD}}/4$. This result cannot be correct, because vanishing adsorption would then imply a rather strong bulk contribution. The wrong result originates from two sources: (a) For very small absorption coefficients of the harmonic wave, the hyperpolarizability depends, due to conservation of energy, on the absorption coefficient α_ω. Using an *ad hoc* ansatz for the hyperpolarizability to be quadratic—with a small coefficient—in α_ω produces the required result that for vanishing absorption of the harmonic the frequency-doubled SHG wave vanishes too. (It also vanishes for linear dependence.) (b) The second reason comes from the assumption of neglecting the phases. This assumption is not justified any more; for propagation lengths of the order of 10 μm, phase (mis)matching (wave vectors $k_\omega, k_{2\omega}$) has to be taken into account in Eq. (4). It will be shown in the following section how the spatial dispersion formulation in Eqs. (3) and (4) can be incorporated in the theoretical framework of Peng *et al.* [12].

III. REFORMULATION OF SPATIAL DISPERSION NONLINEAR CONTRIBUTION

Spatial dispersion in the framework of the SBHM was first discussed using the classical electrodynamics calculation by Peng *et al.* [12]. Using a formal theoretical approach, they show that the various allowed nonlinear contributions and first-forbidden bulk contributions to SHG in centrosymmetric materials can be derived using a Green's-function expression for the four-potential of the radiation from a point charge q which is propagating in free space. The radiated field far-field $\boldsymbol{E}_{ff}$ follows as a special case of the Liénard-Wiechert potentials for an accelerated charge [12]:

$$\boldsymbol{E}_{ff} = \frac{qk^2}{r}(\overleftrightarrow{I} - \hat{k}\hat{k})\cdot\sum\hat{b}_j\left\{\frac{q(\hat{\boldsymbol{b}}_j\cdot\boldsymbol{E}_o)}{\kappa_1 - m\omega^2}e^{ikr-i\omega t}e^{i(\boldsymbol{k}_o-\boldsymbol{k})\cdot\boldsymbol{r}_o} + \frac{q^2(\hat{\boldsymbol{b}}_j\cdot\boldsymbol{E}_o)^2}{(\kappa_1 - m\omega^2)^2(\kappa_1 - 4m\omega^2)}\right.$$
$$\left.\times\,[-i(\hat{\boldsymbol{b}}_j\cdot\boldsymbol{k})(\kappa_1 - 4m\omega^2) + 2i(\hat{\boldsymbol{b}}_j\cdot\boldsymbol{k}_o)(\kappa_1 - m\omega^2) - 2\kappa_2]e^{2ikr-2i\omega t}e^{2i(\boldsymbol{k}_o-\boldsymbol{k})\cdot\boldsymbol{r}_o}\right\}. \tag{5}$$

The first term in braces is the linear optic response, and the remaining three terms describe SHG. The physical origin of the three SHG terms is clear from the development: The first term, which involves the outgoing wave vector, is the electric quadrupole contribution; the second term, which involves the incoming wave vector, arises from spatial dispersion; and the third term, which depends only on the anharmonic restoring force, reduces to the contribution from asymmetric bonding at the interface for SHG from centrosymmetric crystals [12]. The intensity is proportional to the absolute square of the far field after all contributions have been taken into account. The spatial dispersion term in Eq. (5) is

$$\boldsymbol{E}_{ff}^{\mathrm{SD}} = \frac{qk^2}{r}(\overleftrightarrow{I} - \hat{k}\hat{k}) \cdot \sum_{j=1}^{8} \frac{2iq^2 \hat{\boldsymbol{b}}_j (\hat{\boldsymbol{b}}_j \cdot \boldsymbol{E}_o)^2 (\hat{\boldsymbol{b}}_j \cdot \boldsymbol{k}_o)(\kappa_1 - m\omega^2)}{(\kappa_1 - m\omega^2)^2(\kappa_1 - 4m\omega^2)} e^{2ikr - 2i\omega t} e^{2i(\boldsymbol{k}_o - \boldsymbol{k})\cdot \boldsymbol{r}_o}, \tag{6}$$

which can be written more compactly as

$$\begin{aligned} \boldsymbol{E}_{ff}^{\mathrm{SD}} &= S\frac{qk^2}{r}(\overleftrightarrow{I} - \hat{k}\hat{k}) \cdot 2i \sum_{j=1}^{8} \alpha_{\mathrm{SD}} \hat{\boldsymbol{b}}_j (\hat{\boldsymbol{b}}_j \cdot \boldsymbol{E}_o)^2 (\hat{\boldsymbol{b}}_j \cdot \boldsymbol{k}_o) \\ &= S\frac{qk^2}{r}(\overleftrightarrow{I} - \hat{k}\hat{k}) \cdot \sum_{j=1}^{8} \boldsymbol{p}_j^{(\mathrm{SD})}, \end{aligned} \tag{7}$$

where $\alpha_{\mathrm{SD}} = \frac{q^2(\kappa_1 - m\omega^2)}{(\kappa_1 - m\omega^2)^2(\kappa_1 - 4m\omega^2)}$ is the spatial dispersion nonlinear hyperpolarizability which is a function of the incoming frequency ω, S is given by $e^{2ikr-2i\omega t} e^{2i(\boldsymbol{k}_o - \boldsymbol{k})\cdot \boldsymbol{r}_o}$,

$$\begin{aligned} \boldsymbol{p}_j^{(\mathrm{SD})} &= \alpha_{\mathrm{SD}}\, \hat{\boldsymbol{b}}_j (\hat{\boldsymbol{b}}_j \cdot \boldsymbol{E}_o)^2 (\hat{\boldsymbol{b}}_j \cdot \boldsymbol{k}_o) \\ &= \overleftrightarrow{\chi}^{(3)}_{\mathrm{SBHM\text{-}SD}} \cdots \boldsymbol{E}(\omega) \otimes \boldsymbol{E}(\omega) \otimes \boldsymbol{k}_o \end{aligned} \tag{8}$$

is the spatial dispersion nonlinear polarization, and $\overleftrightarrow{\chi}^{(3)}_{\mathrm{SBHM\text{-}SD}}$ is the third-rank spatial dispersion nonlinear susceptibility. Interestingly, Eq. (8) looks very similar to the third equation in Eq. (3), where $\boldsymbol{k}_o$ in the later equation is given by the decaying field gradient term $(C_{(1)} - C_{(2)})$ in the second-order nonlinear SHG spatial dispersion polarization. The slight difference between the results of Peng *et al.* [12] and our results is only in the way in which we look at them. Peng *et al.* take, in our opinion, the whole symmetric charge distribution of two silicon atoms together and declare it as one charge moving along the bond. Then the longitudinal spatial dispersion is due to the fact that this charge distribution moves in a field gradient. In this paper, we analyze the spatial dispersion by looking at two charges, each one sitting in the vicinity of each Si atom, and due to a decaying field in the z direction, we have a noncanceling contribution.

We now proceed by analyzing the tensorial properties of the reformulated spatial dispersion. From the viewpoint of the SBHM, if the sample is allowed to rotate freely along the z axis by an angle of ϕ, then $\overleftrightarrow{\chi}^{(3)}_{\mathrm{SBHM\text{-}SD}}$ takes the form

$$\begin{aligned} \overleftrightarrow{\chi}^{(3)}_{\mathrm{SBHM\text{-}SD}} = \frac{1}{V} \sum_{j=1} \alpha_{\mathrm{SD}} (\mathbf{R}^{(z)} \cdot \hat{\boldsymbol{b}}_j) \otimes (\mathbf{R}^{(z)} \cdot \hat{\boldsymbol{b}}_j) \otimes (\mathbf{R}^{(z)} \cdot \hat{\boldsymbol{b}}_j) \\ \otimes (\mathbf{R}^{(z)} \cdot \hat{\boldsymbol{b}}_j), \end{aligned} \tag{9}$$

where V is the volume, $\hat{\boldsymbol{b}}_j$ are the unit vectors in the direction of the atomic bonds, and $\mathbf{R}^{(z)}$ is the rotation matrix about the z axis. Here, $\hat{\boldsymbol{b}}_j$ are the unit vectors in the direction of the atomic bonds. By inserting the bond vectors and rotational matrix for the Si(100) and Si(111) facets and performing a contraction with the incoming field, one will readily obtain a third-rank tensor containing only one independent parameter, namely, the SHG spatial dispersion hyperpolarizability. This approach is similar to our previous work regarding SHG from an electric-field-induced second harmonic (EFISH) generation [30] in the z direction with only one independent parameter, namely, the spatial dispersion hyperpolarizability complex number. A full derivation of this result with regard to group theory is given in the Appendix.

IV. EXPERIMENTAL EVIDENCE OF SPATIAL DISPERSION IN Si(111)

In this section we focus our discussion on the Si(111) facet orientation instead of Si(001) because in the latter orientation the spatial dispersion contribution is harder to separate from the other sources due to the symmetric fourfold SHG intensity peak feature. The Si(111) bond unit vectors and the defined coordinate systems in the simulation are similar to those in Ref. [21]. Some of the few wavelength-dependent data for a *p*-incoming fundamental, *p*-outgoing wave SHG polarization (which we refer to as *pp* throughout the text) on a nonmiscut Si(111) sample have been measured by Kravetsky *et al.* [37] for three different frequencies at an angle of incidence (AOI) of 45°, as replotted in the left column of Fig. 3. Experimentally, it turns out that the SHG signal is, as a function of the azimuthal angle 0°–360°, either threefold, when the absorption length is small [for a vacuum wavelength of $\lambda_{0,2\omega} =$ 266 nm, Fig. 3(a)] or sixfold, when the absorption length is huge [for a vacuum wavelength of $\lambda_{0,2\omega} = 532$ nm, Fig. 3(c)] [37]. This feature can be easily explained by assuming a bulk contribution in the form of a quadrupole and spatial dispersion contribution. However, as has been shown in the previous discussion, the spatial dispersion contribution can be redefined in the SBHM as similar to a bulk dipolar contribution and is responsible for the different features of the smaller threefold second harmonic (SH) intensity peaks. This is because for low AOI the projection of the field on the three bonds is almost identical, giving a sixfold symmetry: The fundamental wave has an AOI of 45° in air, within the oxide the AOI is $\simeq$29°, and within Si the AOI is, due to its large refractive index, $\leqslant$ 11.3°, depending on the wavelength, where if one takes an AOI = 0°, a perfect sixfold SH intensity pattern is directly obtained.

Furthermore, to reproduce the experimental fit, it has to be noted that the nonlinear SH susceptibility value depends on the incoming (ω) and SH (2ω) frequency as can be seen from Eq. (1). Therefore we apply different parameters for the surface SH nonlinear susceptibility for the three different SHG

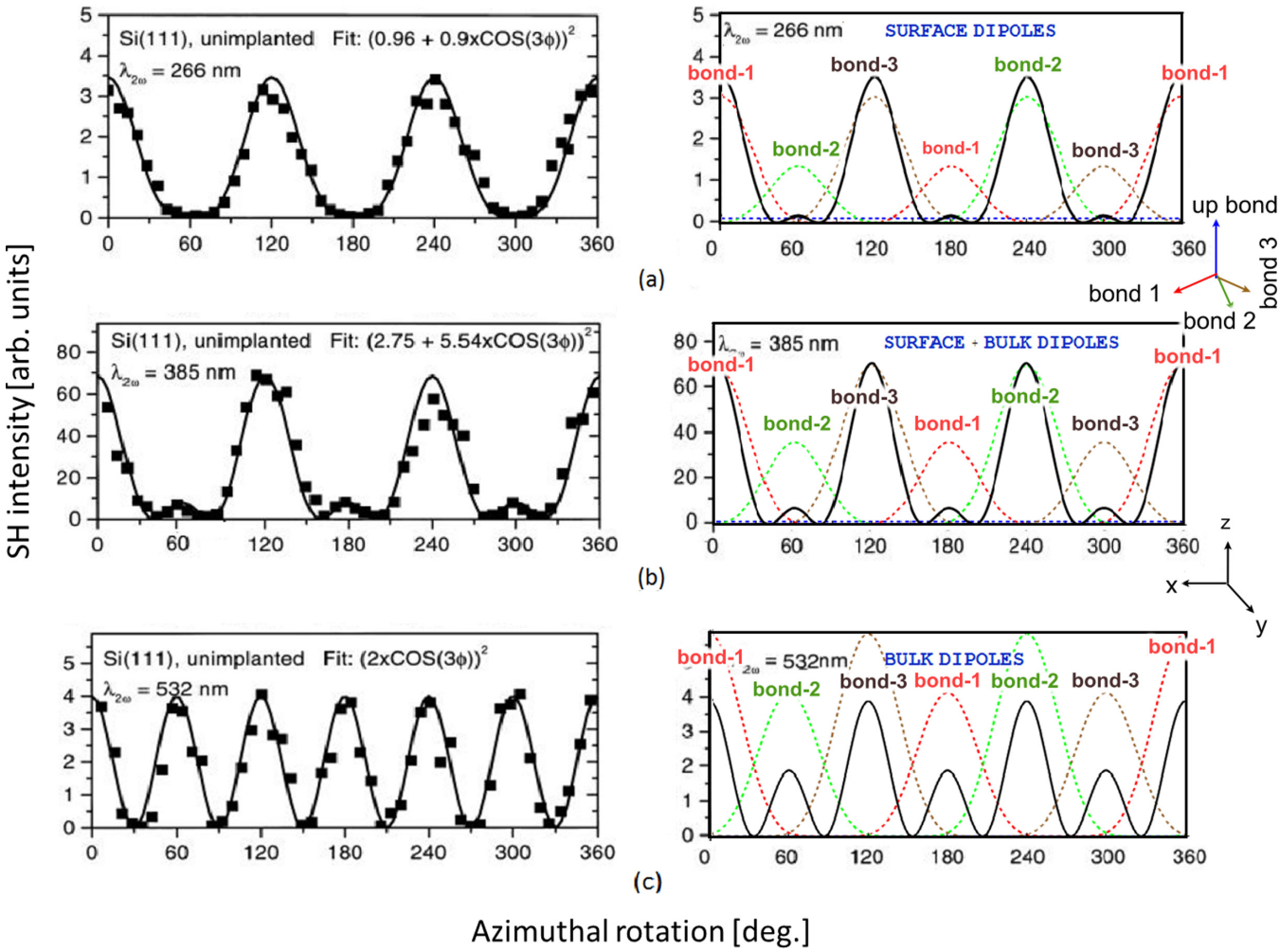

FIG. 3. Left: Measured azimuthal dependence as a function of wavelength [(a) 266 nm, (b) 385 nm, and (c) 532 nm]. Data are replotted (with permission) from Ref. [37]. Right: Simulated SBHM data of one slab using one (bulk) hyperpolarizability and two angles of incidence. For $\lambda_{0,2\omega} = 266$ nm, only an AOI $= 29^\circ$ (SiO_2) was used; for the case of $\lambda_{0,2\omega} = 532$ nm, an AOI $= 11.47^\circ$ for the harmonic wave was used. For $\lambda_{0,2\omega} = 385$ nm a linear combination of AOI $= 29^\circ$ and AOI $= 11.0^\circ$ was used. The total intensity is plotted using black lines, and the intensity from the contributing bonds is given with dashed blue (up bond), red (down bond 1), green (down bond 2), and brown (down bond 3) lines.

frequencies used in fitting Fig. 3 for Si(111) SHG intensity *pp* polarization obtained from Ref. [37]. The values of the nonlinear surface susceptibilities for Si(111) were obtained from Fig. 2(a) in Ref. [38] and were derived using *ab initio* self-consistent tight-binding theory. The values of the SHG nonlinear surface susceptibility $\chi^{(2)}_{zzz}$ for the SH wavelengths of 266, 385, and 532 nm are 15×10^{-19}, 5×10^{-19}, and 3×10^{-19} m^2/V, respectively [38]. In addition, the escape depth and absorption coefficient of the SH radiation for the SH wavelengths of 266, 385, and 532 nm are 5, 40, and 800 nm, respectively [37]. Hence the observed RASHG intensity in Fig. 3(a) corresponding to the SH wave of 266 nm shows very strong surface SH effects since the optical penetration is only 1–2 atomic layers deep and the observed pattern resembles a threefold peak surface Si(111) symmetry in accordance with the C_{3v} point group. For the SH wavelength of $2\omega = 385$ nm the surface nonlinear susceptibility is only 1/3 of that of $2\omega = 266$ nm, and now the optical penetration depth is 40 nm, so bulk effects become significant.

We now modify the SBHM to model SH spatial dispersion from bulk dipoles by assigning different AOIs as explained in the first paragraph of this section. In the SBHM the harmonic polarization is given by $\vec{P}^{2\omega} = \sum_j \beta_{2j} \vec{b}_j \vec{b}_j \vec{b}_j \bullet\bullet \vec{E}\vec{E} = \chi_2 \bullet\bullet \vec{E}\vec{E}$, with the bullets denoting inner tensorial products summing over all bonds j. The hyperpolarizability β_{2j} denotes the nonlinear hyperpolarizability of the Si bond, pointing towards the tetrahedra corners, and is a function of the frequency. Therefore the changes in the nonlinear hyperpolarizability due to frequency are given by a second parameter or onset mimicking the hyperpolarizability strength β_2 to adjust the arbitrary intensity SHG experimental data since we do not know the exact value of β_2 as a function of the frequency. In the right column of Fig. 3 the fits are shown. It turns out that in order to obtain the best fit the change in the bulk hyperpolarizability value for higher SH frequencies has to be adjusted to compensate the changes in the surface dipole offset after considering Fresnel coefficients for the bulk sources.

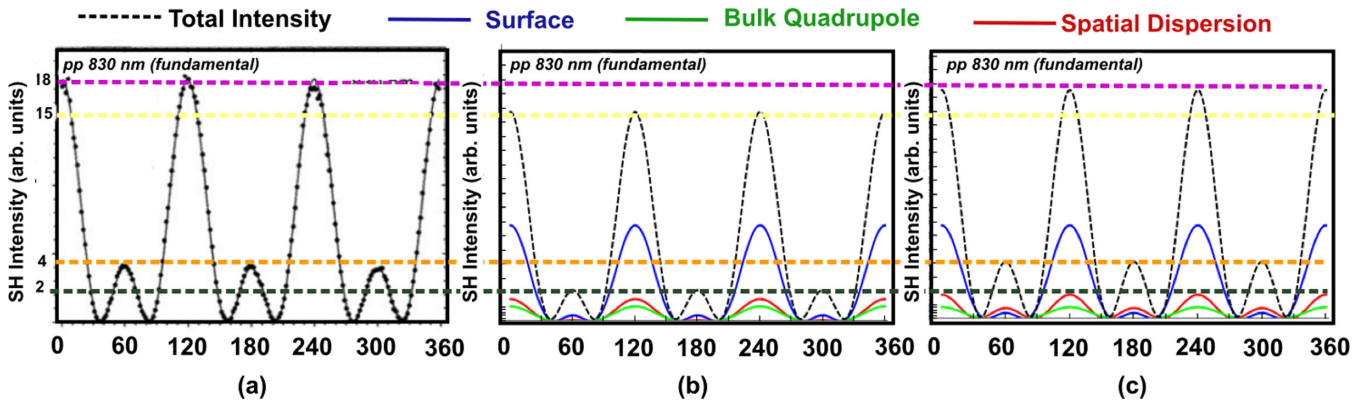

FIG. 4. Comparison between (a) *pp* RASHG intensity polar plot experiment by Mitchell *et al.* [41] for a fundamental incoming wavelength of 830 nm and the corresponding SBHM simulation assuming (b) almost no penetration into the bulk (AOI = 29°) and (c) penetration into the bulk (AOI = 11.3°). The SBHM calculation takes into account the surface contribution (blue lines), bulk quadrupole (green lines), spatial dispersion (red lines), and Fresnel coefficients to produce the total SHG intensity (black dashed lines). The increase in the small threefold SH intensity peak is due to spatial dispersion.

To obtain the exact value of the bulk hyperpolarizability, further investigation is required using *ab initio* models to explore Eq. (1) and introduce a symmetry breaking due to field decay as well as investigate the interactions and the involved transitions. Indeed, one can follow the approach taken by Mendoza and Mochán in Ref. [39], where the macroscopic nonlinear bulk and surface susceptibilities for different frequencies were calculated from the microscopic susceptibility tensors of each bond, yielding good agreement with the experimental work of Aspnes and Studna [40]. We believe that such an approach can also be performed for spatial dispersion involving a bulk field gradient along the optical axis. However, the calculation of nonlinear SH spatial dispersion susceptibility lies beyond the scope of this research, where we focus mainly on the phenomenological aspects of the SBHM and on the reformulation of spatial dispersion from a classical point of view, and we encourage further investigation on this subject.

The modified SBHM now considers the contribution from bulk dipoles from two factors: the radiating dipoles themselves at smaller AOI due to Snell's law and due to changes in the hyperpolarizability (frequency effect). Nevertheless, we believe that the latter effect together with the increase in bulk layers can be a significant factor in explaining the 20-fold SH *pp* intensity increase in Fig. 3(b) and in Fig. 5 of Ref. [39]. In the simulation, we apply an AOI of 45°, as replotted in the left column of Fig. 3. An additional parameter was used to adjust the relative contribution of the surface with AOI = 29°, yielding a mainly threefold symmetry, and of the bulk with AOI $\simeq$ 9°, giving rise to a sixfold symmetry. The SBHM yields for the up bond a baseline shift (plotted in blue), and the contribution of the three down bonds is plotted in red, green, and brown. The total intensity is plotted in black. For $\lambda_{0,2\omega} = 266$ nm, only an AOI = 29° was used, for $\lambda_{0,2\omega} = 532$ nm a pure bulk spatial dispersion contribution was considered, and for the intermediate wavelength $\lambda_{0,2\omega} = 385$ nm a combination of AOI = 29° and AOI = 11.0° was used. The assignments "surface dipoles" and "bulk dipoles" in Fig. 3 stem purely from the different AOIs depending on the different frequency-dependent refractive indices. The fit for $\lambda_{0,2\omega} = 532$ nm shows a symmetric sixfold peak pattern although we have carried out similar RASHG experiments for $\lambda_{0,2\omega} = 445$ nm, which is close to 532 nm, showing a similar threefold pattern [22]. Interestingly, the smaller threefold peak can also be attributed to the relative phase values between the isotropic and anisotropic coefficients a(3) and c(3) in Eq. (76) of Ref. [39] using the polarizable bond model. In this paper we offer an alternative view that this effect can also arise due to spatial dispersion because of the different driving fields experienced by dipoles along the optical axis since the incoming field is absorbed. To support this claim, we calculated the ratios between the high and low SHG *pp* intensity peaks and compared them with existing experimental data, and we obtained a very good match.

Figure 4 shows the SBHM simulation to reproduce the experimental results of Ref. [41] for a very small penetration light depth of 5–10 nm at the interface (AOI = 29°), depicted in Fig. 4(b), and for a higher penetration depth (AOI = 11.3°) corresponding to a Si refractive index of $n = 3.7$ for an incoming wavelength of 830 nm and absorption coefficient of around 760.12 cm^{-1} based on the data reported by Aspnes and Studna [40], as shown in Fig. 4(c). The surface nonlinear hyperpolarizability values corresponding to the involved frequencies were obtained from Ref. [38], and the bulk hyperpolarizabilities were adjusted accordingly. The SBHM simulation considers the contribution from surface dipoles, the contribution from bulk quadrupoles, and the bulk spatial dispersion SHG contribution as well as Fresnel coefficients for the *pp* polarization. The Fresnel coefficients and the hyperpolarizability offsets will be important to obtain a rough estimate of the surface, quadrupole, and spatial dispersion contributions for all possible light polarizations. Because measurements were made using arbitrary SHG intensity units, the ratio between the high threefold peak and low threefold peak is important. For the experiment in Fig. 4(a) the high-peak-to-low-peak ratio is 4.5. Assuming AOI = 29° as shown in Fig. 4(b), the high-peak-to-low-peak ratio is 7.5, which is far from a good fit even if the offset ratios are adjusted or if only surface dipoles (ratio is 35/2.5 = 14) or

bulk quadrupoles (pure threefold) are considered. The best fit with experiment was obtained for an AOI = 11.3°, which matches Snell's law for an incoming wavelength of 830 nm when the surface, quadrupole, and spatial dispersion contribution onset ratio was 2 : 1 : 1, or in other words the surface contribution was two times larger than the quadrupole and spatial dispersion contribution as shown in Fig. 4(c). The spatial dispersion contribution is thus significant to reproduce the best fit.

We found using the SBHM simulation that decreasing the AOI from 29° to 0° gradually corresponds to an increase in the smaller threefold peak SHG intensity, becoming fully sixfold if the AOI is set to zero. The SBHM prediction is observed in the experimental data measured by Kravetsky *et al.* [37], where the threefold small peak for $\lambda_{0,2\omega} = 415$ nm is higher than that for $\lambda_{0,2\omega} = 385$ nm. In addition, our simulation also shows that only the spatial dispersion SHG contribution is responsible for this effect because as shown in Figs. 4(b) and 4(c) the bulk quadrupole (green lines) and surface contribution (red lines) does not alter the threefold peak height. Thus this is the first proof that the SHG spatial dispersion radiation can explain the difference in the variation of the threefold SHG small peak pattern for different incoming wavelengths. However, despite using two bulk-related contributions, namely, spatial dispersion and bulk quadrupole, it is clear to us that the surface contribution will be important for certain surface terminations—and is furthermore frequency dependent [42].

Moreover, we would also state that this model can be applied for a different material, e.g., crystal symmetry [38], by attributing the proper bond vector orientation for the surface and bulk and performing the same procedure, namely, a layer-by-layer analysis as in Eq. (3). In addition, for a transparent material the absorption coefficient is very small, so that the field decay is negligible within the optical penetration depth. Therefore spatial dispersion due to bulk dipole is not significant in this case. For very large absorption, such as the case in Fig. 3(a), the optical penetration depth is only a few nanometers, and spatial dispersion becomes negligible. Furthermore, other Si(111) RASHG experimental data for an incoming *pp* wavelength of 830 nm corresponding to $\lambda_{0,2\omega} = 415$ nm also exist [41] showing a threefold peak pattern similar to our experimental result [22].

To test the absolute surface-versus-bulk SHG contribution ratio, we offer an experimental setup that can also be useful to determine the strength of spatial dispersion. Despite there having been proposals in the literature [20,43], e.g., using steps to separate the "pure" bulk and surface contributions, we propose one unambiguous technique, separating the harmonic and frequency-doubled signals in space. The proposal works for (slightly) dispersive materials and makes use of the different propagation directions inside the material of the harmonic and frequency-doubled reflection. Just using the Huygens principle of constructing the planes of equal phase for $\vec{E}_\omega$ and $\vec{E}_{2\omega}$ (see Fig. 5), one can determine experimentally the bulk SHG contribution by cutting a Si crystal (e.g., with a focused ion beam) in a shape as shown. Such a geometry allows one to let the $\vec{E}_{2\omega}$ field pass through the interface without undergoing refraction (but certainly weakened by the effect). The radiating $\vec{E}_\omega$, however, is refracted to increasing angles.

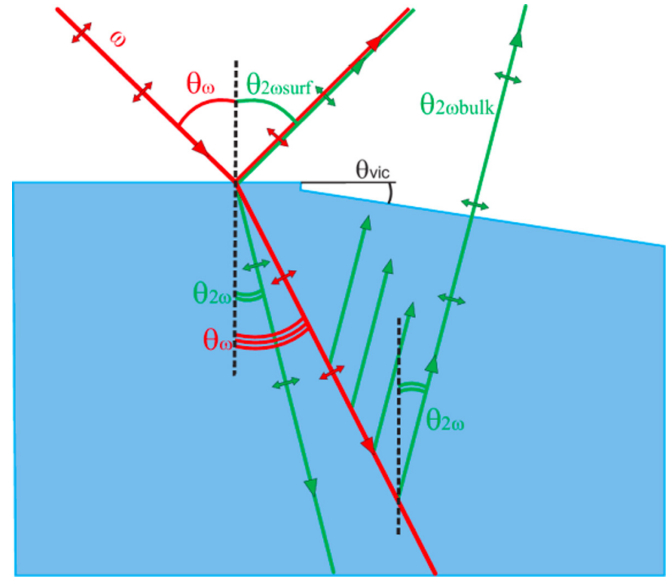

FIG. 5. Proposed geometry for measuring unambiguously the dipolar bulk contribution of SHG. For a harmonic wave of 1064 nm ($n = 3.64$) with an AOI = 45° and a SHG frequency of 532 nm ($n = 4.14$, penetration depth 1.3 μm) and for θ_{vic} of 9.8° the SHG wave passes the vicinal surface without being refracted ($\theta_{\text{bulk}} = 0$). However, the harmonic wave is refracted at 5.8° to the right. Therefore the frequency-doubled wave, which contains surface and bulk contributions, is approximately 35° separated from the field only containing the bulk contribution.

V. SUMMARY

Summarizing, we show that in the diamond structure, a spatial dispersion SHG response can exist if two atoms, establishing a symmetric entity, experience different field strengths and thereby the radiated harmonic field does not fully cancel. The dipole-allowed bulk SHG spatial dispersion originates then due to the finite absorption length of the electric field in the material. Analysis of the spatial dispersion nonlinear polarization and tensorial properties shows that the theoretical formulation of Peng *et al.* [12] regarding spatial dispersion in the form of a third-order nonlinear SHG effect can be reformulated in terms of a second-order SHG effect using a reduced third-rank nonlinear spatial dispersion susceptibility with only one independent parameter in the tensor. Furthermore, our SBHM simulation shows that the spatial dispersion contribution is roughly half and equal to the surface dipole and bulk quadrupole contribution, respectively, yielding an excellent fit only if spatial dispersion is included in the SBHM. However, an exact comparison can only be obtained if the nonlinear bulk hyperpolarizabilities can be calculated from *ab initio* models, and further work in this area is encouraged. Finally, we compare our simulation results with available wavelength-dependent SHG data, whose azimuthal dependence can be

well modeled, and propose a measurement scheme capable of unambiguously separating bulk and surface effects.

ACKNOWLEDGMENTS

H.H. would like to thank the Hibah Kompetensi Grant No. 3989/IT3.L1/PN/20 (20/21) and Program Penugasan WCU 2021 of Kemenristek Dikti, A.A.-M. would like to thank the Mexican National Council of Science and Technology (CONACyT) for financial support during this research (under Contract No. CB-2015-01/254617). The work of H.A. is partially funded by World Class Research (WCR) Grant form the Directorate of Higher Education, Indonesian Ministry of Education and Culture. H.H. would like to especially thank Kurt Hingerl for the stimulating discussions and help. We thank David Stifter, Cornelia Reitboeck, Norbert Esser and Siegfried Bauer for valuable comments on the manuscript.

APPENDIX

The bond direction of the Si bonds is defined by following the convention from standard crystallographic tables for the conventional diamond cell [44,45]. For the Si(100) orientation the bond unit vector directions are

$$\hat{\boldsymbol{b}}_1 = \begin{pmatrix} -\frac{1}{\sqrt{2}}\sin\frac{\beta}{2} \\ -\frac{1}{\sqrt{2}}\sin\frac{\beta}{2} \\ -\cos\frac{\beta}{2} \end{pmatrix}, \quad \hat{\boldsymbol{b}}_2 = \begin{pmatrix} \frac{1}{\sqrt{2}}\sin\frac{\beta}{2} \\ \frac{1}{\sqrt{2}}\sin\frac{\beta}{2} \\ -\cos\frac{\beta}{2} \end{pmatrix},$$
$$\hat{\boldsymbol{b}}_3 = \begin{pmatrix} -\frac{1}{\sqrt{2}}\sin\frac{\beta}{2} \\ \frac{1}{\sqrt{2}}\sin\frac{\beta}{2} \\ -\cos\frac{\beta}{2} \end{pmatrix}, \quad \hat{\boldsymbol{b}}_4 = \begin{pmatrix} \frac{1}{\sqrt{2}}\sin\frac{\beta}{2} \\ -\frac{1}{\sqrt{2}}\sin\frac{\beta}{2} \\ \cos\frac{\beta}{2} \end{pmatrix} \tag{A1}$$

with opposing bonds

$$\hat{\boldsymbol{b}}_5 = -\hat{\boldsymbol{b}}_1, \quad \hat{\boldsymbol{b}}_6 = -\hat{\boldsymbol{b}}_2, \quad \hat{\boldsymbol{b}}_7 = -\hat{\boldsymbol{b}}_3, \quad \hat{\boldsymbol{b}}_8 = -\hat{\boldsymbol{b}}_4. \tag{A2}$$

By substituting the bond definitions in Eqs. (A1) and (A2) into Eq. (9) and evaluating β we obtain the following matrix:

$$\overleftrightarrow{\chi}^{(3)}_{\text{SBHM-SD}} = \frac{\alpha_{\text{SD}}}{V} \begin{pmatrix} \begin{pmatrix} \frac{4}{9}[3-\cos(4\phi)] & -\frac{4}{9}\sin(4\phi) & 0 \\ -\frac{4}{9}\sin(4\phi) & \frac{8}{9}\cos^2(2\phi) & 0 \\ 0 & 0 & 0 \end{pmatrix} & \begin{pmatrix} -\frac{4}{9}\sin(4\phi) & \frac{8}{9}\cos^2(2\phi) & 0 \\ \frac{8}{9}\cos^2(2\phi) & \frac{4}{9}\sin(4\phi) & 0 \\ 0 & 0 & 0 \end{pmatrix} & \begin{pmatrix} 0 & 0 & \frac{8}{9} \\ 0 & 0 & 0 \\ \frac{8}{9} & 0 & 0 \end{pmatrix} \\ \begin{pmatrix} -\frac{4}{9}\sin(4\phi) & \frac{8}{9}\cos^2(2\phi) & 0 \\ \frac{8}{9}\cos^2(2\phi) & \frac{4}{9}\sin(4\phi) & 0 \\ 0 & 0 & 0 \end{pmatrix} & \begin{pmatrix} \frac{8}{9}\cos^2(2\phi) & \frac{4}{9}\sin(4\phi) & 0 \\ \frac{4}{9}\sin(4\phi) & \frac{4}{9}[3-\cos(4\phi)] & 0 \\ 0 & 0 & \frac{8}{9} \end{pmatrix} & \begin{pmatrix} 0 & 0 & 0 \\ 0 & 0 & \frac{8}{9} \\ 0 & \frac{8}{9} & 0 \end{pmatrix} \\ \begin{pmatrix} 0 & 0 & \frac{8}{9} \\ 0 & 0 & 0 \\ \frac{8}{9} & 0 & 0 \end{pmatrix} & \begin{pmatrix} 0 & 0 & 0 \\ 0 & 0 & \frac{8}{9} \\ 0 & \frac{8}{9} & 0 \end{pmatrix} & \begin{pmatrix} \frac{8}{9} & 0 & 0 \\ 0 & \frac{8}{9} & 0 \\ 0 & 0 & \frac{8}{9} \end{pmatrix} \end{pmatrix}. \tag{A3}$$

Setting $\phi = 0$, the tensor simplifies to

$$\overleftrightarrow{\chi}^{(3)}_{\text{SBHM-SD}} = \frac{8\alpha_{\text{SD}}}{9V} \begin{pmatrix} \begin{pmatrix} 1 & 0 & 0 \\ 0 & 1 & 0 \\ 0 & 0 & 1 \end{pmatrix} & \begin{pmatrix} 0 & 1 & 0 \\ 1 & 0 & 0 \\ 0 & 0 & 0 \end{pmatrix} & \begin{pmatrix} 0 & 0 & 1 \\ 0 & 0 & 0 \\ 1 & 0 & 0 \end{pmatrix} \\ \begin{pmatrix} 0 & 1 & 0 \\ 1 & 0 & 0 \\ 0 & 0 & 0 \end{pmatrix} & \begin{pmatrix} 1 & 0 & 0 \\ 0 & 1 & 0 \\ 0 & 0 & 1 \end{pmatrix} & \begin{pmatrix} 0 & 0 & 0 \\ 0 & 0 & 1 \\ 0 & 1 & 0 \end{pmatrix} \\ \begin{pmatrix} 0 & 0 & 1 \\ 0 & 0 & 0 \\ 1 & 0 & 0 \end{pmatrix} & \begin{pmatrix} 0 & 0 & 0 \\ 0 & 0 & 1 \\ 0 & 1 & 0 \end{pmatrix} & \begin{pmatrix} 1 & 0 & 0 \\ 0 & 1 & 0 \\ 0 & 0 & 1 \end{pmatrix} \end{pmatrix}. \tag{A4}$$

If we assume for the sake of simplicity that the incoming p-polarized field is directed normal to the sample or along the z axis, we have $\boldsymbol{k}_o = (0, 0, 1)$, and then we can contract the spatial dispersion tensor $\overleftrightarrow{\chi}^{(3)}_{\text{SBHM}-\text{SD}}$ with $\boldsymbol{k}_o = (0, 0, E_z)$ so that for this special case the third-order spatial dispersion tensor reduces to a second-order nonlinear tensor, which is obviously the third column of the tensor elements in Eq. (A4).

$$\overleftrightarrow{\chi}^{(2)}_{\text{SBHM-SD}} = \frac{8\alpha_{\text{SDeff}}}{9V}\begin{pmatrix}\begin{pmatrix}0&0&1\\0&0&0\\1&0&0\end{pmatrix}\\\begin{pmatrix}0&0&0\\0&0&1\\0&1&0\end{pmatrix}\\\begin{pmatrix}1&0&0\\0&1&0\\0&0&1\end{pmatrix}\end{pmatrix}. \tag{A5}$$

The second-order tensor above is similar to the tensor obtained from group theory (GT), where for Si the bulk point group is O_h and a field gradient due to spatial dispersion along the z axis will cause the symmetry to break into a lower symmetry similar to the Si(001) surface, which is C_{2v} and takes the form

$$\overleftrightarrow{\chi}^{(2)}_{\text{GT-SD}} = \begin{pmatrix}\begin{pmatrix}0&0&s_{3232}\\0&0&0\\s_{3322}&0&0\end{pmatrix}\\\begin{pmatrix}0&0&0\\0&0&s_{3232}\\0&s_{3322}&0\end{pmatrix}\\\begin{pmatrix}s_{3223}&0&0\\0&s_{3223}&0\\0&0&s_{3333}\end{pmatrix}\end{pmatrix}. \tag{A6}$$

Equation (A6) is a 3×3 matrix whose elements are also a 3×3 matrix. The first index "i'' corresponds to the rows in the principal matrix, whereas the indices "j'' and "k'' correspond to the rows and columns in the internal 3×3 matrices. For the the case of SHG, the two fundamental driving fields are indistinguishable, so we can apply intrinsic permutation $s_{3322} = s_{3232}$. Furthermore, assuming symmetry in the diagonal of the contracted matrix representation, we have $s_{3223} = s_{3232}$, and again both the spatial dispersion and SHG second-order tensor now only require two independent parameters.

Analogously, if the incoming field is s polarized, then $\boldsymbol{k}_o = (0, 1, 0)$, and in this case we have

$$\overleftrightarrow{\chi}^{(2)}_{\text{SBHM-SD}} = \frac{8\alpha_{\text{SDeff}}}{9V}\begin{pmatrix}\begin{pmatrix}0&1&0\\1&0&0\\0&0&0\end{pmatrix}\\\begin{pmatrix}1&0&0\\0&1&0\\0&0&1\end{pmatrix}\\\begin{pmatrix}0&0&0\\0&0&1\\0&1&0\end{pmatrix}\end{pmatrix}. \tag{A7}$$

A similar approach can be taken for different Si facet orientations. For the case of Si(111) we first apply a rotation on the (001) matrix about the z axis and evaluate the tensor at $\phi = \pi/4$, labeled $\mathbf{R}^{(z)}(\pi/4)$. Afterwards, a second transformation about the x axis for an angle of $\beta/2$ is applied, which we label as $\mathbf{R}^{(x)}(\beta/2)$. After applying these transformations and contracting with a unitary vector along the z axis, the resulting effective third-rank tensor for the Si(111) orientation is

$$\overleftrightarrow{\chi}^{(2)}_{\text{SBHM-SD}} = \frac{8\alpha_{\text{2effSD}}}{27V}\begin{pmatrix}\begin{pmatrix}0&-\sqrt{2}&1\\-\sqrt{2}&0&0\\1&0&0\end{pmatrix}\\\begin{pmatrix}-\sqrt{2}&0&0\\0&\sqrt{2}&1\\0&1&0\end{pmatrix}\\\begin{pmatrix}1&0&0\\0&1&0\\0&0&7\end{pmatrix}\end{pmatrix}, \tag{A8}$$

which again shows that in the SBHM the third-rank tensor describing spatial dispersion requires only one independent parameter, which is the second-order effective spatial dispersion hyperpolarizability. The tensor in Eq. (A8) is similar to the GT tensor for a symmetry breaking of the point group O_h into C_{3v}.

[1] J. E. Sipe, D. J. Moss, and H. M. van Driel, Phys. Rev. B **35**, 1129 (1987).
[2] V. Mizrahi and J. E. Sipe, J. Opt. Soc. Am. B **5**, 660 (1988).
[3] N. Arzate and B. S. Mendoza, Phys. Rev. B **63**, 113303 (2001).
[4] B. Gokce, E. J. Adles, D. E. Aspnes, and K. Gundogdu, Proc. Natl. Acad. Sci. U. S. A. **107**, 17503 (2010).
[5] C. Schriever, C. Bohley, and R. B. Wehrspohn, Opt. Lett. **35**, 273 (2010).
[6] M. Cazzanelli, F. Bianco, E. Borga, G. Pucker, M. Ghulinyan, E. Degoli, E. Luppi, V. Veniard, S. Ossicini, D. Modotto, S. Wabnitz, R. Pierobon, and L. Pavesi, Nat. Mater. **11**, 148 (2012).
[7] J. F. McGilp, J. Phys.: Condens. Matter **22**, 084018 (2010).
[8] K. Sahu, K. B. Eisenthal, and V. F. McNeill, J. Phys. Chem. C **115**, 9701 (2011).
[9] F. X. Wang, F. J. Rodriguez, W. M. Albers, R. Ahorinta, J. E. Sipe, and M. Kauranen, Phys. Rev. B **80**, 233402 (2009).
[10] P. Guyot-Sionnest and Y. R. Shen, Phys. Rev. B **38**, 7985 (1988).
[11] W. S. Kolthammer, D. Barnard, N. Carlson, A. D. Edens, N. A. Miller, and P. N. Saeta, Phys. Rev. B **72**, 045446 (2005).
[12] H. J. Peng, E. J. Adles, J.-F. T. Wang, and D. E. Aspnes, Phys. Rev. B **72**, 205203 (2005).
[13] M. Corvi and W. L. Schaich, Phys. Rev. B **33**, 3688 (1986).
[14] G. D. Powell, J.-F. Wang, and D. E. Aspnes, Phys. Rev. B **65**, 205320 (2002).
[15] R. W. Boyd, *Nonlinear Optics* (Academic, New York, 2003).
[16] Y. R. Shen, Nature (London) **337**, 519 (1989).
[17] N. Bloembergen, R. K. Chang, S. S. Jha, and C. H. Lee, Phys. Rev. **174**, 813 (1968).

[18] E. J. Adles and D. E. Aspnes, Phys. Status Solidi A **205**, 728 (2008).
[19] J. A. Litwin, J. E. Sipe, and H. M. van Driel, Phys. Rev. B **31**, 5543 (1985).
[20] J. F. McGilp, J. Phys.: Condens. Matter **19**, 016006 (2007).
[21] H. Hardhienata, A. Prylepa, D. Stifter, and K. Hingerl, J. Phys.: Conf. Ser. **423**, 012046 (2013).
[22] C. Reitböck, D. Stifter, A. Alejo-Molina, K. Hingerl, and H. Hardhienata, J. Opt. (Bristol) **18**, 035501 (2016).
[23] C. Reitböck, D. Stifter, A. Alejo-Molina, H. Hardhienata, and K. Hinger, Appl. Surf. Sci. **421**, 761 (2017).
[24] K.-D. Bauer, M. Panholzer, and K. Hingerl, Phys. Status Solidi B **253**, 234 (2016).
[25] H. Hardhienata, A. Alejo-Molina, C. Reitböck, A. Prylepa, D. Stifter, and K. Hingerl, J. Opt. Soc. Am. B **33**, 195 (2016).
[26] H. Hardhienata, I. Priyadi, H. Alatas, M. D. Birowosuto, and P. Coquet, J. Opt. Soc. Am. B **36**, 1127 (2019).
[27] H. Hardhienata, I. Priyadi, B. Nurjanati, and H. Alatas, J. Nonlinear Opt. Phys. Mater. **27**, 1850025 (2018).
[28] A. Alejo-Molina, H. Hardhienata, and K. Hingerl, J. Opt. Soc. Am. B **31**, 526 (2014).
[29] E. S. Jatirian-Foltides, J. J. Escobedo-Alatorre, P. A. Marquez-Aguilar, H. Hardhienata, K. Hingerl, and A. Alejo-Molina, Rev. Mex. Fis. E **62**, 5 (2016).
[30] A. Alejo-Molina, K. Hingerl, and H. Hardhienata, J. Opt. Soc. Am. B **32**, 562 (2015).
[31] G. New, *Introduction to Nonlinear Optics* (Cambridge University Press, Cambridge, 2011).
[32] G. Kresse and D. Joubert, Phys. Rev. B **59**, 1758 (1999).
[33] B. Gokce, K. Gundogdu, E. J. Adls, and D. E. Aspnes, J. Korean Phys. Soc. **58**, 1237 (2011).
[34] V. Agranovich and V. Ginzburg, *Spatial Dispersion in Crystal Optics and the Theory of Excitons*, Interscience Monographs and Texts in Physics and Astronomy Vol. 18 (Interscience, New York, 1966).
[35] J. E. Mejia, C. Salazar, and B. S. Mendoza, Rev. Mex. Fis. **50**, 134 (2004).
[36] H. Fearn, D. F. V. James, and P. W. Milonni, Am. J. Phys. **64**, 986 (1996).
[37] I. Kravetsky, L. Kulyuk, J. McGilp, M. Cavanagh, S. Chandola, J. Boness, G. Marowsky, and F. Harbsmeier, Surf. Sci. **402–404**, 542 (1998).
[38] V. I. Gavrilenko and F. Rebentrost, Appl. Phys. A: Mater. Sci. Process. **60**, 143 (1995).
[39] B. S. Mendoza and W. L. Mochán, Phys. Rev. B **55**, 2489 (1997).
[40] D. E. Aspnes and A. A. Studna, Phys. Rev. B **27**, 985 (1983).
[41] S. A. Mitchell, R. Boukherroub, and S. Anderson, J. Phys. Chem. B **104**, 7668 (2000).
[42] S. Mitchell, M. Mehendale, and D. Villeneuve, Surf. Sci. **488**, 367 (2001).
[43] G. Lüpke, D. J. Bottomley, and H. M. van Driel, J. Opt. Soc. Am. B **11**, 33 (1994).
[44] J. F. Nye, *Physical Properties of Crystals: Their Representation by Tensors and Matrices* (Oxford University Press, New York, 1985).
[45] R. C. Powell, *Symmetry, Group Theory, and the Physical Properties of Crystals* (Springer-Verlag, New York, 2010).